Automated Laser Ultrasonic NDT of Carbon Fibre Reinforced Polymer Parts

Martin GAERTNER [1], Bernhard REITINGER [1], Wolfgang HADERER[1], Bernhard PLANK [2], Johann KASTNER [2], Juergen GRUBER [2], Guenther MAYR [2], Vicki JAMES [3], Peter BURGHOLZER [1], Edgar SCHERLEITNER [1]

[1] Research Center for Non Destructive Testing GmbH, Altenberger-Str. 69, 4040 Linz, AT
[2] University of Applied Sciences of Upper Austria, Stelzhamer-Str. 23, 4600 Wels, AT
[3] TWI Technology Centre Wales, Harbourside Business Park, Port Talbot, SA13 1SB, UK

e-mail: martin.gaertner@recendt.at

Abstract
We present the application and the results of laser ultrasonic scanning systems on fibre-based composites and the current state of development of this method at RECENDT. First we benchmark this technique with X-ray tomography and infrared thermography and then show a robotized scanning system dedicated for the aerospace industry. The laser ultrasonic systems use a 532 nm Nd:YAG pulsed laser for excitation and a 1064 nm two-wave-mixing interferometer for detection. The fibre coupling enables a flexible scan head for the automation of the system. The laser ultrasonic technique is demonstrated on a sample with artificial defects, such as PTFE-foils as a delamination source. The results are compared with reference NDT-methods such as X-ray computed tomography and active thermography, and the individual advantages and disadvantages are discussed. Further, a robotised scanning system will be presented, which has been developed under the H2020 Clean Sky 2 project ACCURATe. The sampling rate of this system is 400 Hz, which enables large parts to be inspected at the required speed. A large aircraft part made of carbon fibre reinforced polymer was manufactured and investigated for real world defect measurements.

Keywords: Laser ultrasound, active infrared thermography, X-ray computed tomography, time of flight (TOF), aerospace, carbon fibre reinforced polymer (CFRP), NDT, composite

1. Introduction

Carbon fibre reinforced polymer (CFRP) is widely used for lightweight products. The respective production processes are still rather complex, manual and error-prone, which is why the strictly regulated aerospace industry in particular demands effective non-destructive testing methods. State-of-the-art techniques are X-ray computed tomography (XCT), water-coupled ultrasound testing and infrared active thermography (IRT), which was recently approved as new method by Boeing. We want to introduce laser ultrasound (LUS) as powerful alternative and compare it with existing NDT-methods, each of which has its individual advantages and disadvantages. Water-coupled ultrasound is not investigated in this study, as wetting of the sample should be avoided.
We will present two use cases to show the potential of LUS. First, a comparison of a LUS scan with XCT and IRT on a CFRP sample plate with artificially induced delaminations by PTFE (Polytetrafluoroethylene) -foils. Second, the functionality of a fibre-coupled and robotised LUS system is demonstrated on a realistic sample of the aircraft industry.

2. Applied laser ultrasound method

In the case of LUS, the generation and detection of ultrasonic waves are performed by a contactless method by the use of lasers [1][2]. The principle of the applied laser ultrasonic method is indicated in Figure 1. In order to achieve high signal amplitudes, the excitation laser is adjusted to operate in both, the thermoelastic [3] and ablative regime [4]. The incident laser

beam penetrates the material (<0.5 mm) and causes a local, rapid increase in temperature and an expansion of a small volume followed by cooling. This thermoelastic process excites compressional and shear waves which are typically in the frequency range of 1 MHz to 10 MHz. The additional ablative process generates ultrasound by the abrupt evaporation of traces of the surface (<1 µm), which causes ultrasonic pressure waves mainly perpendicular to the surface. For detection a two-wave-mixing interferometer (TWM) [5] with a photorefractive crystal and a balanced photo detector is used. The detection laser has a pulse length of 80-100 µs, a wavelength of 1064 nm, and a spot diameter of 1 mm, see Figure 1 (red laser beam).

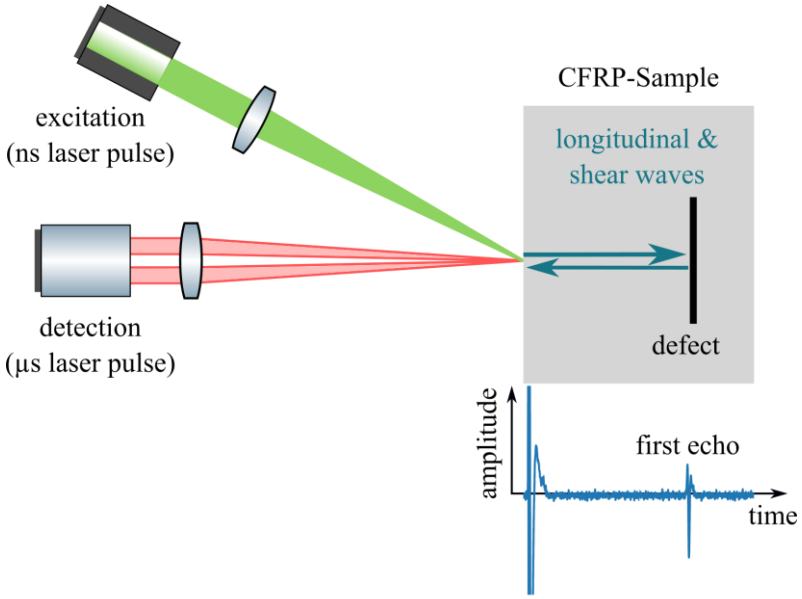

Figure 1. Laser ultrasonic configuration used in the measurement head for detection of a delamination in a carbon fibre reinforced polymer (CFRP) sample.

3. Comparison of methods on CFRP sample

The CFRP-sample used is approximately 200x160x6 mm^3 in size. The plate has a glossy side and a matt side, hereinafter referred to as the front and the back side, respectively. It contains 15 artificially induced flaws made of PTFE-foil. The size of the flaws varies from 5x5 mm^2 to 25x25 mm^2, which are introduced at depths from 1 mm to 5 mm. Figure 2 shows a sketch of the sample plate with the exact locations and size of the artificial defects (left) and a photo of the front side of the plate (right).

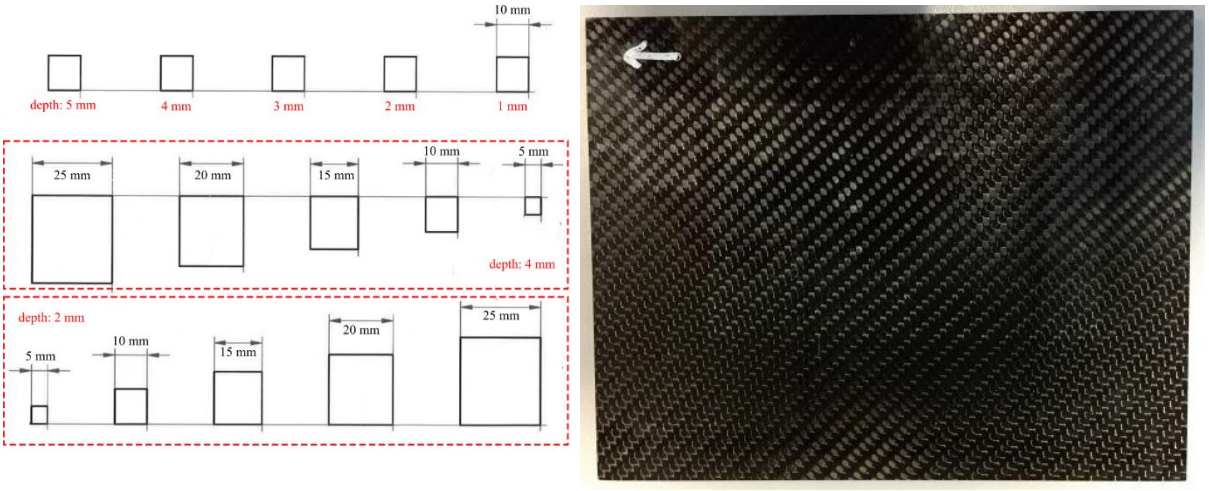

Figure 2. Sketch of the sample plate, 6 mm thick, with the locations and sizes of the artificial defect (left) and photo of the front side of the plate (right).

3.1 Laser ultrasonic measurements

The laser ultrasonic testing of the plate was performed in reflexion mode. For the excitation a flash lamp pumped and frequency doubled Nd:YAG laser at 532 nm from InnoLas was used. The laser had a pulse length of approximately 5 ns and ran at a repetition rate of 100 Hz. The laser was aligned in a free space setup and focused with an approximate spot size of 2 mm on the sample. The pulse energy was set at 15 mJ which allowed us to work in the thermoelastic regime and not to destroy the sample.
For the detection of the ultrasonic waves a pulsed detection laser (PDL) from Tecnar was used. It operates at 100 Hz and 1064 nm with a pulse length of 100 µs. The demodulation of the ultrasonic signals was performed by a balanced two wave mixing interferometer working with a photorefractive GaAs crystal. For the automation of the measurement, two stages were used to move the sample according the meander scan path with steps of 0.5 mm x 0.5 mm.
Figure 3 show the results of the LUS measurements where the time of flight of each pulse is colour coded, i.e. a so called “time-of-flight” (TOF) image. One can intuitively associate the defects with their corresponding depths. In the C-scan (Figure 4 left) all 6 flaws in depth of 2 mm are visible. On the right-hand of Figure 4 the C-scan in a depth of 6 mm (backwall) shows all echoes accumulated in one image.
The pattern in the LUS images results from the different absorption properties of the surface due to the carbon fibre structure, see Figure 2 (right). This artefact could be reduced if the surface variations in absorption were taken into account by signal processing.

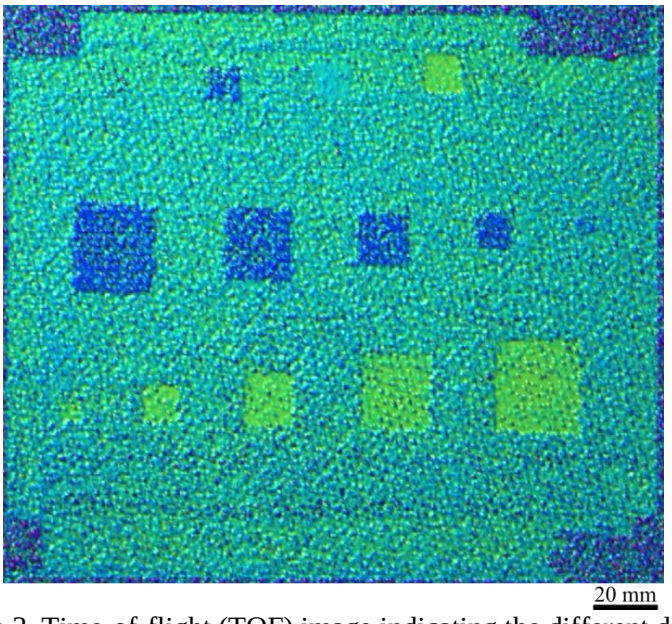

Figure 3. Time-of-flight (TOF) image indicating the different depths.

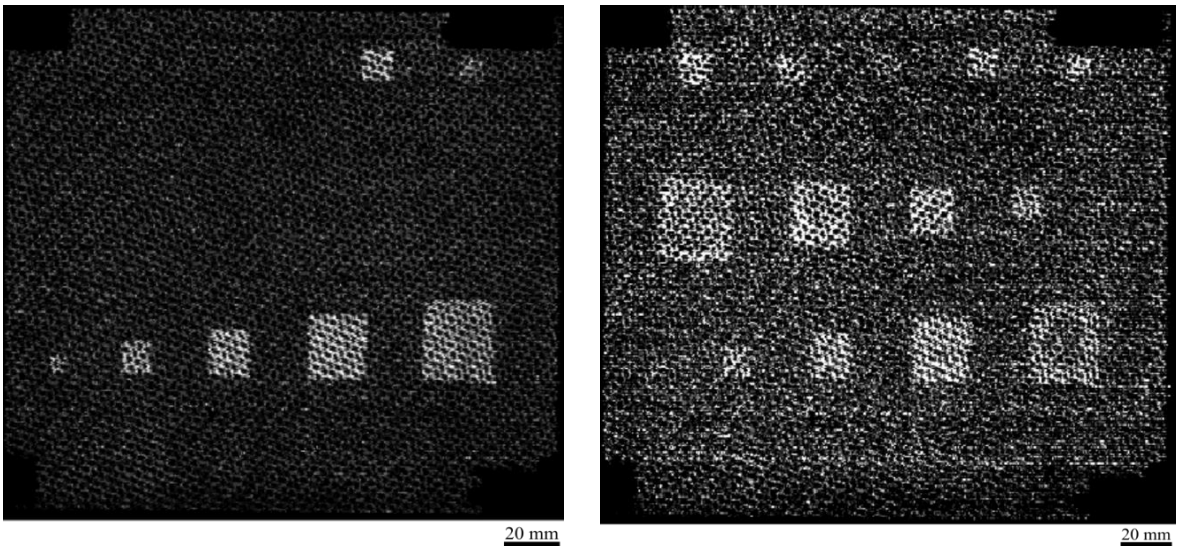

Figure 4. LUS C-scan in depths of 2 mm (left) and 6 mm (backwall), where all echoes accumulated in the image (right).

3.2 Reference measurements

3.2.2 Active Thermography

For the plates evaluation by means of active thermography testing was performed in reflexion and in transmission mode. For the thermal excitation two flash lamps, each with an electrical energy of 6 kJ, were positioned to achieve a strong and homogeneous illumination of the plates. To filter the longwave afterglow of the flash lamps two sheets of acrylic glass were set in front of the flash lamps. The temperature field on the plate's surface was recorded with the infrared camera FLIR X8400sc for 200 s with the frame rate set to 25 Hz. The plate fills measurement window of 640x512 px almost entirely which corresponds to an optical resolution of approximately $\frac{\mathbf{610}\boldsymbol{px}}{\mathbf{200}\boldsymbol{mm}} = \mathbf{3.05}\,\frac{\boldsymbol{px}}{\boldsymbol{mm}}$.

For evaluation in the time domain the diffusion time $\boldsymbol{t_d}$ was calculated for each pixel using the TSR-method [6], for reflexion mode measurements and the LDF-method [7] for transmission mode measurements. For a constant thickness $\boldsymbol{l}$ this parameter corresponds to the thermal diffusivity $\boldsymbol{\alpha} = \frac{\boldsymbol{l^2}}{\boldsymbol{t_d}}$, which is affected by the defects.

In the frequency domain, phase contrast images were calculated by applying the Fourier transform [8] to both reflexion mode and transmission mode data.

Figure 5 shows the resultant images of the time domain evaluation. In comparison to reflexion mode measurements it can be clearly seen that transmission mode measurements are able to detect almost every artificial defect with sufficient contrast. However transmission mode setup requires access from both sides of the sample plate.

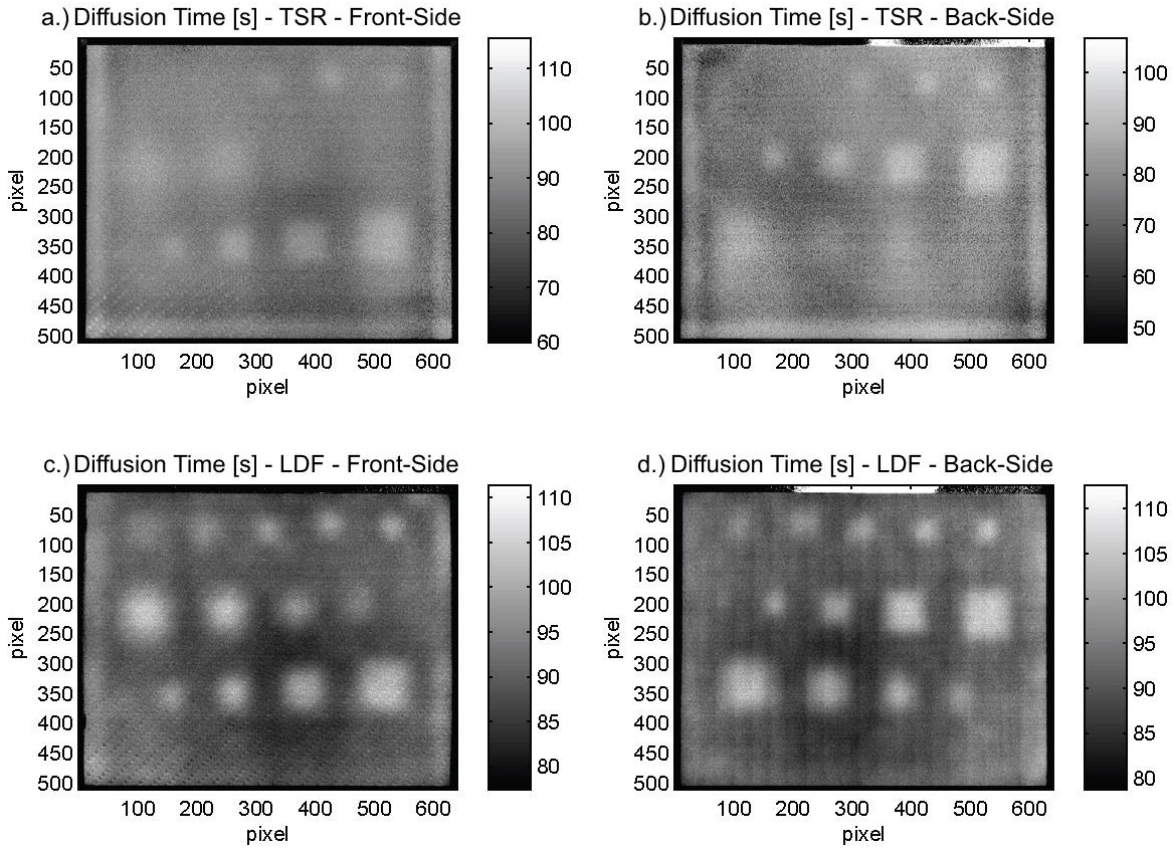

Figure 5. Comparison of diffusion time images calculated from reflexion mode measurements by using the TSR-method for (a) front- and (b) back-side and from transmission mode measurements by using the LDF-method for (c) front- and (d) back-side.

Figure 6 exemplarily shows the phase contrast images at 0.06 Hz for transmission mode measurements carried out at the Front- and Back side. As can be seen almost all artificial defects could be detected. Phase contrast images gained from reflexion mode measurements require evaluation at different frequencies due to the varying depth of the artificial defects. For reasons of compactness we have decided not to include phase contrast images from reflexion mode measurements.

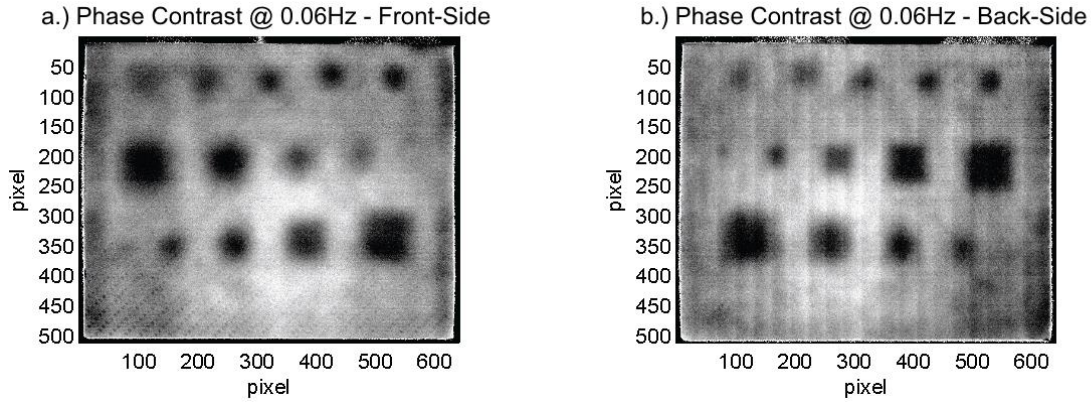

Figure 6. Phase contrast images @ 0.06Hz calculated from the transmission mode measurement for (a) front- and (b) back-side.

3.2.3 X-ray computed tomography

The X-ray computed tomography (XCT) scan was performed on a RayScan 250E (RayScan Technologies GmbH, Meersburg, Germany), equipped with a 225 kV microfocus and a 450 kV minifocus X-ray tube which was also equipped with a 2048² pixel flat panel-detector.
For the given plate sample size an edge length of a volumetric pixel (voxel size) of 125 µm³ was achieved. The microfocus tube was operated at a tube voltage of 180 kV, using a current of 330 µA. During one complete rotation of the sample 1800 projection images were taken with an integration time of 1999 ms resulting in a total measurement time of 125 min.
Figure 7 shows the XCT results in terms of individual slice images (left, bottom) as well as a 3D image (right) after manual segmentation of the artificial defects. Thus, the artificial defects are on different layers, on one x-z slice image only defects (brighter grey values) are represented on the same layer, clearly resolving the exact dimensions of the flaws ranging from 5x5 mm² up to 25x25 mm². In the shown x-y slice, the depth of each individual 10x10 mm² flaw in the top row can be observed as follows: 1.3, 2.1, 2.9 3.7 and 4.5 mm below the surface, which is very close to the values in Figure 2, whereby the production process of the sample was not able to guarantee the intended values exactly, i.e. 1, 2, 3, 4, 5 mm. Additional grey value gradients for example bright areas on the very left and right of the slice images as well darker areas around the artificial defects are mainly results of XCT reconstruction artefacts, such as Feldcamp artefacts as well as beam hardening artefacts. The rotation axis for this XCT scan was in x-direction.
The 3D image on the right showing all visible defects in the specimen, coloured by their projected area in x-z plane, ranging from ~25 mm² (blue) up to ~625 mm² (red).

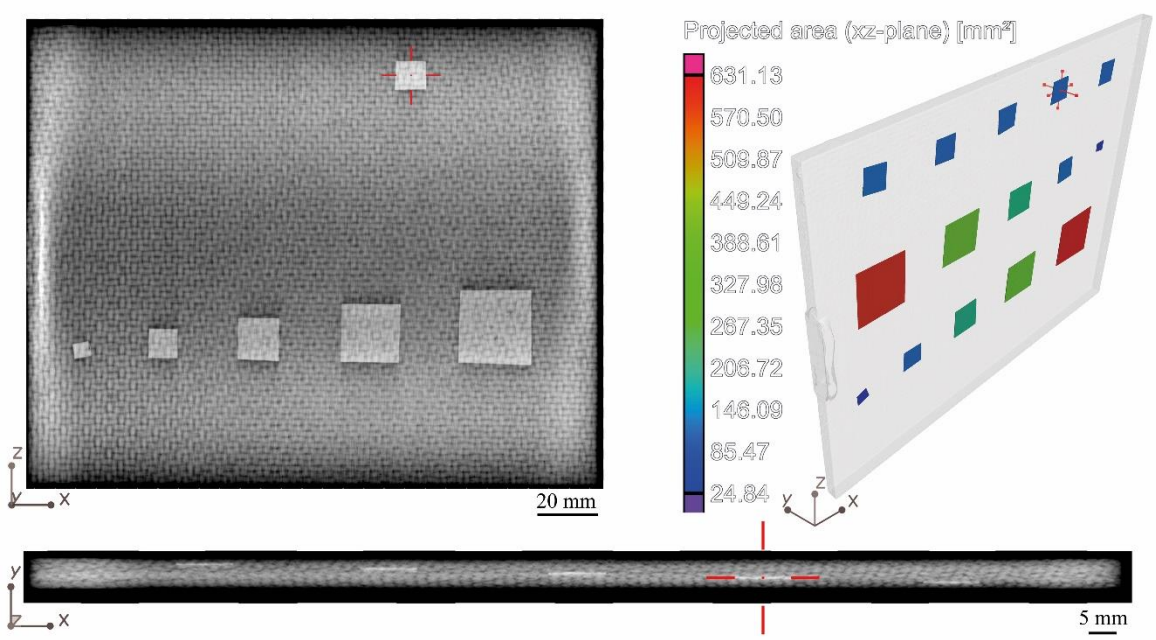

Figure 7. XCT slice images in x-z (left) and x-y direction (bottom) as well a 3D rendering of all segmented flaws showing the projected area size in x-z plane.

3.2.3 Discussion of results

All investigated methods, i.e. LUS, IRT and XCT, show good correlation to the intended position and shape of the delaminations as shown in Figure 2, whereby the XCT results give more accurate depths values as the manufacturing process of the sample was manual and the depths of the PTFE-foils were hard to set exactly. The achievable lateral resolution for LUS on thin samples is mainly governed by the step size of the x-y-scan and the spot diameter of the detection laser. Thus, in the present case the lateral resolution is about 0.5 mm. Similar to XCT, LUS provides C-scans with a depth resolution (depending on the evaluated ultrasonic frequency range), as can be seen comparing the LUS result in Figure 4 (left) and XCT image in Figure 7 which are in excellent agreement. The lateral resolution of IRT decreases rapidly with depth, with the detection limit at most reaching the point where the depth is equal to the defect diameter if no special reconstruction technique is used [9]. The measurement times depend on the specific settings of the systems. The scan duration of LUS (in this case 21 min) scales with the step size and the repetition rate of the lasers, for IRT (3.3 min) it depends on the speed of the thermal diffusion process, the need for averaging and the frame rate of the IR camera, and for XCT (125 min) it depends on the number of required projection images.

4. Robotised laser ultrasound scanning system

The ACCURATe (Aerospace Composite Components Ultrasonic Robot Assisted Testing) project is a European funded H2020 CLEANSKY 2 project. The aim is to develop a non-destructive testing system for fast and contactless testing of large CFRP aircraft structures. A 6 axis Kuka robot moving on a linear track is used to scan large structures. The area coverage is approximately 1.5x1.5 m^2 from a single location of the robot base. To achieve the desired scan rates of at least 8 m^2 per hour the robot moves with speeds of up to 1.2 m/s.
Two diode pumped Nd:YAG lasers were developed by InnoLas for the laser ultrasonic testing. The detection laser used was a special build 80 µs long pulsed laser at 1064 nm. The excitation laser was a 10 ns short pulse laser at 532 nm. Each laser had a pulse energy of 30 mJ and ran with 400 Hz repetition rate. The laser pulses were provided via optical fibres to the measurement head mounted at the end of the robot arm. The measurement head also included focusing and light collecting optics. Figure 8 shows the Kuka robot with the measurement head scanning a large and curved CFRP sample.
The demodulation of the ultrasonic signals was performed by a balanced two wave mixing interferometer working with a photorefractive GaAs crystal. All measurement data is recorded by a data acquisition card and post processed with special ACCURATe software from TWI which also controls the whole laser system.

4.1 Results

To test the system a CS2 demonstrator with artificially introduced flaws was produced. It contained 125 different types of flaws. They vary in size (from 0.25x0.25 in^2 to 0.7x0.7 in^2), Material (peel ply, PTFE, tape) and depth. Some regions also contain an acoustical veil. Figure 9 shows a full time of flight scan of the CS2 panel. The scanned section of the CS2 panel contains 99 flaws whereof we can visually see 75. This corresponds to 75% of the flaws. The LUS measuring method suffered a challenge detecting the defects in the areas with the acoustical veil (mid-section, right side). These areas are difficult for all ultrasonic examinations, because the damping material strongly attenuates the sound amplitudes which leads to low amplitude signals which are difficult to detect beyond the natural system noise. Using post

processing i.e. histogram filtering (see Figure 10) helps to visually detect more flaws in areas with acoustical veil.

Figure 8. LUS scanning system with Kuka robot and CFRP test panel with realistic flaws.

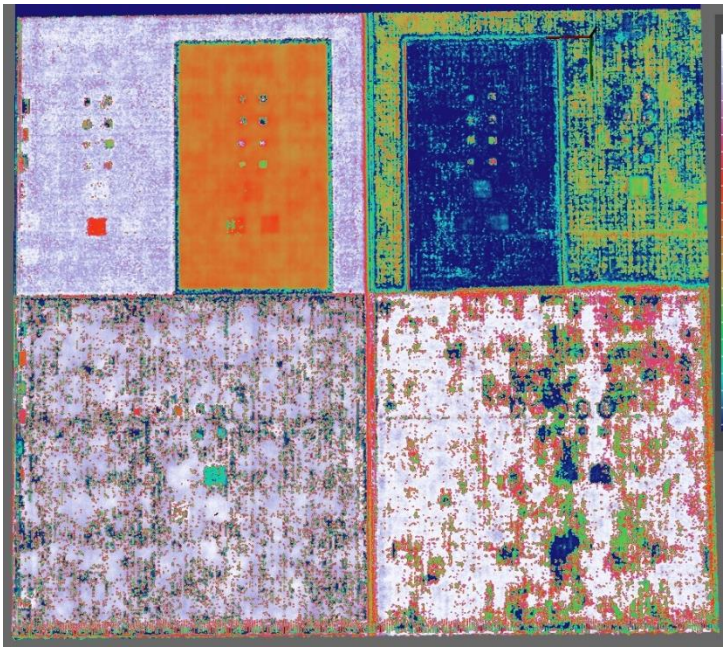

Figure 9. Time of flight scan of CS2 panel with detection laser power of 20W and a robot speed of 0.4m/s.

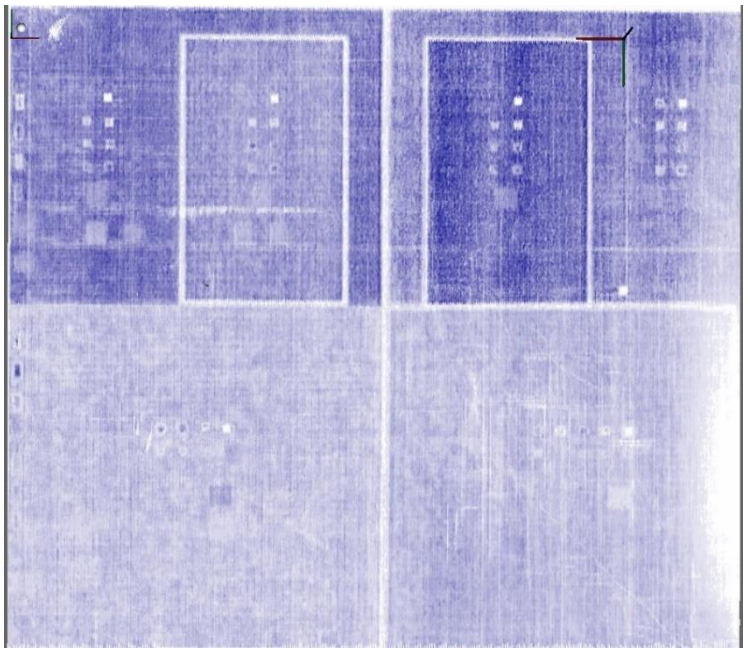

Figure 10. Histogram filtering function of scan result of CS2 panel with detection laser power of 20W and a robot speed of 0.4m/s.

5. Conclusion

We have demonstrated that LUS is a well suited test method for CFRP, in particular, especially when the ability to detect relevant defects, the measurement speed, and automation capabilities in a comparison with IRT and XCT are taken into account. The hardware of appropriate LUS systems [11] has advanced over the last decade in terms of costs, reliability and system footprint, and is now attractive to the automotive and aerospace industries. The technology and methods of IRT could also achieve significant progress. Accordingly, in the field of production of safety-critical components, FACC received Boeing's qualification for IRT testing. As expected from recent investigations [12], for the given sample size of 200x160x6 mm^3 (chapter 3) XCT leads to the best results in terms of resolution in x and z as well as in y direction (sample thickness) with the limitation that the resolution of XCT strongly depends on the specimen size (voxel size scales with field of view and the image matrix). In addition, the maximum specimen size feasible for XCT usually strongly depends on the used XCT-devices. An advantage for LUS and IRT are the lower equipment costs compared to XCT including the consideration of the X-ray radiation safety regulations, whereby LUS is operating class 4 lasers and requires the installation of laser safety shielding. Based on the presented promising results, further research and development targeted at improved LUS hardware and methods for CFRP testing systems is planned, where XCT [14] and IRT [13] will be needed as most important methods for reference and benchmark.

Acknowledgments

This work has been supported by the project ACCURATe of the programme H2020-EU.3.4.5.4.-ITD Airframe (755616), also by the project “multimodal and in-situ characterization of inhomogeneous materials” (MiCi) by the federal government of Upper Austria and the European Regional Development Fund (EFRE) in the framework of the EU-program IWB2020. Furthermore, this work was supported by the strategic economic- research program "Innovative Upper Austria 2020" of the province of Upper Austria. Financial support was also provided by the Austrian research funding association (FFG) under the scope of the

COMET programme within the research project “Photonic Sensing for Smarter Processes (PSSP)” (contract number 871974). This programme is promoted by BMK, BMDW, the federal state of Upper Austria and the federal state of Styria, represented by SFG. XCT evaluations were performed within the project ‘Interpretation and evaluation of defects in complex CFK structures based on 3D-XCT data and structural simulation - (DigiCT-Sim project number: 862015)’ funded by the State Government of Upper Austria and Austrian Research Promotion Agency (FFG).

References

[1] C. B. Scruby and L. E. Drain, *Laser Ultrasonic Testing and Applications*. Bristol, 1990.

[2] J. P. Monchalin *et al.*, “Laser-ultrasonics: from the laboratory to the shop floor,” *Adv. Perform. Mater.*, vol. 5, no. 1–2, pp. 7–23, 1998.

[3] A. G. Every, Z. N. Utegulov, and I. A. Veres, “Laser thermoelastic generation in metals above the melt threshold,” *J. Appl. Phys.*, vol. 114, no. 20, 2013.

[4] T. W. Murray and J. W. Wagner, “Laser generation of acoustic waves in the ablative regime,” *J. Appl. Phys.*, vol. 85, no. 4, pp. 2031–2040, 1999.

[5] S. Zamiri, M. Salfinger, M. Gruber, M. Stückler, and B. Reitinger, “Photorefractive Ultrasonic Sensor for Weld Quality Monitoring,” *Open Access Libr. J.*, vol. 4, pp. 1–11, 2017.

[6] S. M. Shepard, “Reconstruction and enhancement of active thermographic image sequences,” *Opt. Eng.*, vol. 42, no. 5, p. 1337, May 2003.

[7] G. Hendorfer, G. Mayr, G. Zauner, M. Haslhofer, and R. Pree, “Quantitative determination of porosity by active thermography,” in *AIP Conference Proceedings*, 2007, vol. 894, no. 1, pp. 702–708.

[8] T. Chady and K. Goracy, “Evaluation of fiber reinforced polymers using active infrared thermography system with thermoelectric cooling modules,” *AIP Conf. Proc.*, vol. 1949, pp. 4–7, 2018.

[9] G. Mayr, P. Burgholzer, G. Stockner, and G. Hendorfer, “Virtual wave concept for thermal non-destructive evaluation of delamination in composites,” *Proc. 12th ECNDT*, pp. 1–2, 2018.

[10] M. Spies, H. Rieder, J. Bamberg, and B. Henkel, “On- and offline ultrasonic characterization and inspection of additively manufactured components,” *55th Annu. Conf. Br. Inst. Non-Destructive Testing, NDT 2016*, pp. 328–336, 2016.

[11] R. Seyrkammer, S. Zamiri, B. Reitinger, R. Galos, C. Hofer, and P. Burgholzer, “Laser ultrasound investigations on composites with optical generation from visible to infrared,” *19th World Conf. Non-Destructive Test. 2016 (WCNDT), 13 - 17 June 2016, Munich, Ger.*, pp. 1–7, 2016.

[12] H. Kastner, Johann; Christoph, *Handbook of Advanced Non-Destructive Evaluation “X-Ray Tomography.”* 2019.

[13] G. Mayr, B. Plank, J. Sekelja, and G. Hendorfer, “Active thermography as a quantitative method for non-destructive evaluation of porous carbon fiber reinforced polymers,” *NDT E Int.*, vol. 44, no. 7, pp. 537–543, Nov. 2011.

[14] B. Plank, F. Ellert, J. Gruber, C. Gusenbauer, and J. Kastner, “Detection of defects in carbon fiber reinforced polymers by means of visual inspection, ultrasonic testing, digital radiography, active thermography and X-ray computed tomography.,” in *DGZfP Annual Conference 2013*, 2013, p. 9.